Enhanced power generation in concentrated photovoltaics using broadband antireflective coverglasses with moth eye structures

Young Min Song,[1] Yonkil Jeong,[2] Chan Il Yeo,[1] and Yong Tak Lee[1,2,3,4,*]

[1]*School of Information and Mechatronics, Gwangju Institute of Science and Technology, 1 Oryong-dong, Buk-gu, Gwangju 500-712, South Korea*
[2]*Research Institute for Solar and Sustainable Energies, Gwangju Institute of Science and Technology, 1 Oryong-dong, Buk-gu, Gwangju 500-712, South Korea*
[3]*Department of Photonics and Applied Physics, Gwangju Institute of Science and Technology, 1 Oryong-dong, Buk-gu, Gwangju 500-712, South Korea*
[4]*Department of Nanobio Materials and Electronics, Gwangju Institute of Science and Technology, 1 Oryong-dong, Buk-gu, Gwangju 500-712, South Korea*
*ytlee@gist.ac.kr

Abstract: We present the effect of broadband antireflective coverglasses (BARCs) with moth eye structures on the power generation capability of a sub-receiver module for concentrated photovoltaics. The period and height of the moth eye structures were designed by a rigorous coupled-wave analysis method in order to cover the full solar spectral ranges without transmission band shrinkage. The BARCs with moth eye structures were prepared by the dry etching of silver (Ag) nanomasks, and the fabricated moth eye structures on coverglass showed strongly enhanced transmittance compared to the bare glass with a flat surface, at wavelengths of 300 - 1800 nm. The BARCs were mounted on InGaP/GaAs/Ge triple-junction solar cells and the power conversion efficiency of this sub-receiver module reached 42.16% for 196 suns, which is a 7.41% boosted value compared to that of a module with bare coverglass, without any detrimental changes of the open circuit voltages (V_{oc}) and fill factor (FF).

OCIS codes: (040.5350) Photovoltaic; (050.6624) Subwavelength structures; (220.4241) Nanostructure fabrication; (310.6805) Theory and design.

References and links

1. R. M. Swanson, "The promise of Concentrators," Prog. Photovolt. Res. Appl. **8**(1), 93–111 (2000).
2. G. Zubi, J. L. Bernal-Agustin, and G. V. Fracastoro, "High concentration photovoltaic systems applying III-V cell," Renew. Sustain. Energy Rev. **13**(9), 2645–2652 (2009).
3. D. Friedman, "Progress and challenges for next-generation high-efficiency multijunction solar cells," Curr. Opin. Solid State Mater. Sci. **14**(6), 131–138 (2010).
4. M. Yamaguchi, "III-V compound multi-junction solar cells: present and future," Sol. Energy Mater. Sol. Cells **75**(1-2), 261–269 (2003).
5. W. Guter, J. Schone, S. P. Philipps, M. Steiner, G. Siefer, A. Wekkeli, E. Welser, E. Oliva, A. W. Bett, and F. Dimroth, "Current-matched triple-junction solar cell reaching 41.1% conversion efficiency under concentrated sunlight," Appl. Phys. Lett. **94**(22), 223504 (2009).
6. S. P. Philipps, G. Peharz, R. Hoheisel, T. Hornung, N. M. Al-Abbadi, F. Dimroth, and A. W. Bett, "Energy harvesting efficiency of III-V triple-junction concentrator solar cells under realistic spectral conditions," Sol. Energy Mater. Sol. Cells **94**(5), 869–877 (2010).
7. W. H. Southwell, "Gradient-index antireflection coatings," Opt. Lett. **8**(11), 584–586 (1983).
8. J.-Q. Xi, M. F. Schubert, J. K. Kim, E. F. Schubert, M. Chen, S.-Y. Lin, W. Liu, and J. A. Smart, "Optical thin-film materials with low refractive index for broadband elimination of Fresnel reflection," Nat. Photonics **1**, 176–179 (2007).
9. M. F. Schubert, F. W. Mont, S. Chhajed, D. J. Poxson, J. K. Kim, and E. F. Schubert, "Design of multilayer antireflection coatings made from co-sputtered and low-refractive-index materials by genetic algorithm," Opt. Express **16**(8), 5290–5298 (2008).
10. S. J. Jang, Y. M. Song, C. I. Yeo, C. Y. Park, J. S. Yu, and Y. T. Lee, "Antireflective property of thin film a-Si solar cell structures with graded refractive index structure," Opt. Express **19**(S2 Suppl 2), A108–A117 (2011).

#172541 - $15.00 USD Received 23 Aug 2012; revised 21 Sep 2012; accepted 25 Sep 2012; published 15 Oct 2012

11. S. Chattopadhyay, Y.-F. Huang, Y.-J. Jen, A. Ganguly, K.-H. Chen, and L.-C. Chen, "Anti-reflecting and photonic nanostructures," Mater. Sci. Eng. Rep. **69**(1-3), 1–35 (2010).
12. R. Brunner, O. Sandfuchs, C. Pacholski, C. Morhard, and J. Spatz, "Lessons from nature: biomimetic subwavelength structures for high-performance optics," Laser Photon. Rev. **5**, 1–19 (2011).
13. Y.-F. Huang, S. Chattopadhyay, Y.-J. Jen, C.-Y. Peng, T.-A. Liu, Y.-K. Hsu, C.-L. Pan, H.-C. Lo, C. H. Hsu, Y. H. Chang, C.-S. Lee, K.-H. Chen, and L.-C. Chen, "Improved broadband and quasi-omnidirectional anti-reflection properties with biomimetic silicon nanostructures," Nat. Nanotechnol. **2**(12), 770–774 (2007).
14. Y. M. Song, E. S. Choi, J. S. Yu, and Y. T. Lee, "Light-extraction enhancement of red AlGaInP light-emitting diodes with antireflective subwavelength structures," Opt. Express **17**(23), 20991–20997 (2009).
15. Y. M. Song, S. J. Jang, J. S. Yu, and Y. T. Lee, "Bioinspired parabola-shaped subwavelength structures for improved broadband antireflection," Small **6**(9), 984–987 (2010).
16. H. Sai, H. Fujii, K. Arafune, Y. Ohshita, Y. Kanamori, H. Yugami, and M. Yamaguchi, "Wide-Angle Antireflection Effect of Subwavelength Structures for Solar Cells," Jpn. J. Appl. Phys. **46**(6A), 3333–3336 (2007).
17. P. Yu, C.-H. Chang, C.-H. Chiu, C.-S. Yang, J.-C. Yu, H.-C. Kuo, S.-H. Hsu, and Y.-C. Chang, "Efficiency enhancement of GaAs photovoltaics employing antireflective indium tin oxide nanocolums," Adv. Mater. (Deerfield Beach Fla.) **21**(16), 1618–1621 (2009).
18. K. Peng, Y. Xu, Y. Wu, Y. Yan, S. T. Lee, and J. Zhu, "Aligned single-crystalline Si nanowire arrays for photovoltaic applications," Small **1**(11), 1062–1067 (2005).
19. E. C. Garnett and P. Yang, "Silicon nanowire radial p-n junction solar cells," J. Am. Chem. Soc. **130**(29), 9224–9225 (2008).
20. Y. Kojima and T. Kato, "Nanoparticle formation in Au thin films by electron-beam-induced dewetting," Nanotechnology **19**(25), 255605 (2008).
21. Y. M. Song, H. J. Choi, J. S. Yu, and Y. T. Lee, "Design of highly transparent glasses with broadband antireflective subwavelength structures," Opt. Express **18**(12), 13063–13071 (2010).
22. H. Sai, Y. Kanamori, K. Arafune, Y. Ohshita, and M. Yamaguchi, "Light trapping effect of submicron surface textures in crystalline Si solar cells," Prog. Photovolt. Res. Appl. **15**(5), 415–423 (2007).
23. J. Nelson, *The Physics of Solar Cells* (Imperical College Press, 2003).

1. Introduction

Concentrated photovoltaic (CPV) systems with III-V based multi-junction solar cells have been considered a promising form of solar power generation due to their high power conversion efficiency per unit area [1–3]. Other attractive features, such as higher photon absorption by the direct bandgap energies, strong durability against high temperature, and a variety of material selection, also make III-V solar cells very competitive for the space and terrestrial market [4]. A key challenge for CPV technology is light management, which is implemented both by tuning the materials' bandgap and by reducing light reflection at each interface, in a broad solar spectral range. By stacking absorbing materials of different bandgaps (i.e., GaInP/(In)GaAs/Ge cells), III-V multi-junction solar cells currently can absorb light from 300 nm to 1800 nm [5, 6]. Standard single or double layer antireflection (AR) coatings are clearly unsuitable for this type of solar cell due to the limited spectral and angular bandwidth; hence, broadband antireflection layers are necessary in order to improve the power conversion efficiency. In particular, for CPV systems, these AR layers should be designed to minimize reflection at the sub-receiver module level, which contains coverglasses and encapsulants.

Broadband and omni-directional AR characteristics can be realized in this manner by using multi-layered thin film coatings of materials with a gradually varying refractive index [7–10], or through nano-patterning with a tapered profile, creating the so called moth eye structure [11–17]. Many approaches to produce nanostructures with this moth eye effect were successfully developed on various organic/inorganic materials [11, 12], and some of those structures were applied on the surface of solar cells to minimize reflection over the broad wavelength range [16, 17]. However, structures directly integrated on the cell surface could lead to severe surface recombination [16, 18, 19], which degrades the cell performance, or require complex and time consuming fabrication schemes.

Herein, we present an approach to improve the power conversion efficiency of III-V based CPV systems by using broadband antireflective coverglasses (BARCs) with moth eye structures. The use of BARCs provides i) enhanced external quantum efficiency, due strongly to the reduced reflection; ii) a way of integrating the moth eye structures without changing any fabrication procedure at the device level; and iii) no electrical characteristic degradation

#172541 - $15.00 USD Received 23 Aug 2012; revised 21 Sep 2012; accepted 25 Sep 2012; published 15 Oct 2012

because of the electrically separated schemes of the moth eye structures from the solar cells. The moth eye structure was fabricated on the coverglasses by using thermally dewetted Ag nanoparticles (NPs) [14, 20]. The design rules for the moth eye structure were optimized to have AR properties over the entire solar spectral range (300 nm to 1800 nm) through optical modeling by a rigorous coupled-wave analysis (RCWA) method. The AR properties of BARCs were characterized by transmittance spectra measurement and confirmed by cell efficiency measurement of the CPV sub-receiver modules, with BARCs both at one sun and high concentration conditions.

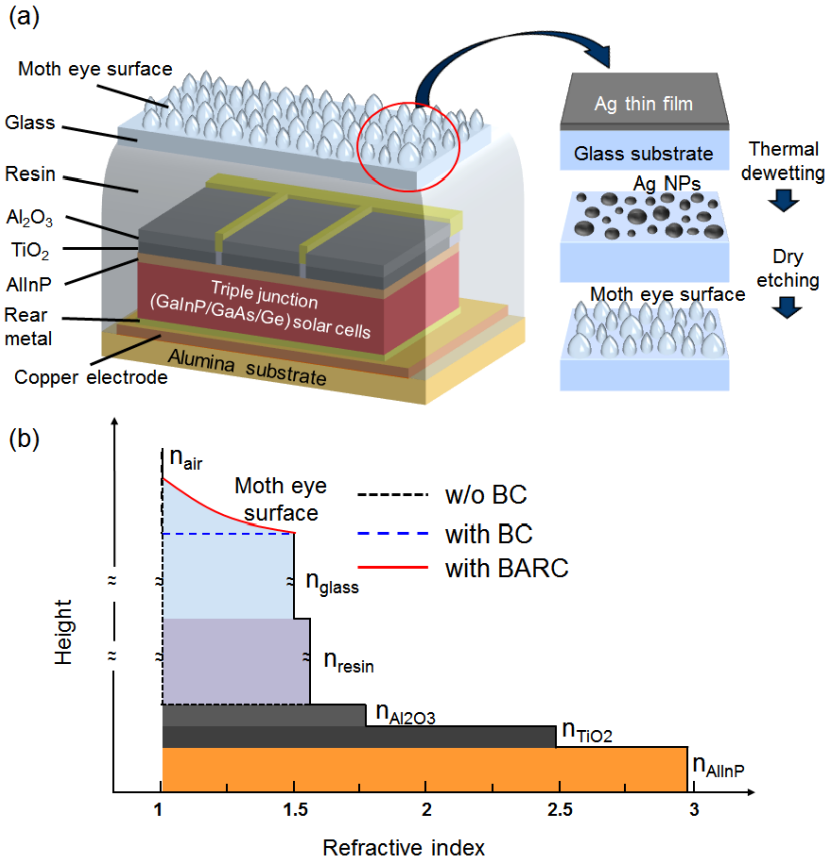

Fig. 1. (a) Schematic diagram of CPV sub-receiver module with BARCs. The right figure shows the fabrication steps for BARCs with moth eye surfaces, (b) Refractive index profiles of CPV sub-receiver module as a function of height for three different cases: without bare coverglass (BC), with BC, and with BARC. Refractive indices of each material at ~600 nm were considered.

2. Experimental details

Figure 1(a) illustrates the basic structure of the III-V based CPV sub-receiver module with BARCs. InGaP/GaAs/Ge triple-junction solar cells (active area = 0.3025 cm^2) with TiO_2/Al_2O_3 double layer AR coatings were used in this experiment. The solar cells are mounted on an alumina substrate with gold-plated thick copper electrode. Then, the cells were encapsulated by a silicone resin and the BARCs were attached on the top of the resin by subsequent hardening with thermal treatment. The steps of BARCs fabrication are depicted in the right image of Fig. 1(a). First, Ag thin films with 10, 20 and 30 nm thickness were deposited on the coverglass substrates (BoroFloat33, Schott) through e-beam evaporation with a deposition rate of 1.0Å/s. To form Ag NPs, the samples were heated in a rapid thermal

#172541 - $15.00 USD Received 23 Aug 2012; revised 21 Sep 2012; accepted 25 Sep 2012; published 15 Oct 2012

annealing (RTA) system at 500 °C for 1 min in a nitrogen environment. To fabricate moth eye structures, an overall dry etch process was carried out in an inductively coupled plasma reactive ion etch (ICP-RIE) system with a CF_4/O_2 (40 sccm/10 sccm) gas mixture at room temperature. The process pressure and RF power were kept at 50 mTorr and 150 W, respectively. The residual Ag NPs were removed by immersion in a wet etchant (KI: I_2: H_2O = 1: 1: 40) that does not affect the shape of the moth eye structure. The surface morphology of the fabricated BARCs was characterized by a field-emission scanning electron microscope (FE-SEM, Hitachi S-4700). The transmittance spectra of each sample were evaluated using an UV-VIS-NIR spectrophotometer (Cary 500, Varian) in the wavelength range of 300 - 2400 nm.

For comparison, three different types of sub-receiver module (i. e., without bare coverglass (BC), with BC, and with BARC) were prepared. As described in Fig. 1(b), in a sub-receiver module without BC (black dashed line), the refractive index changes abruptly from ~2.98 (AlInP, outermost layer of triple-junction solar cells) to 1.0 (air) via only two step grading. The silicone resin (n_{resin}~1.53) and the coverglass (n_{glass}~1.50) slightly relax this abrupt index change (blue dashed line), but an index discontinuity still exists between glass and air. In contrast, the use of the moth eye surface (red solid line) makes an almost linearly graded effective refractive index profile at the interface between the glass and air, which provides efficient light transmission. The current density-voltage (J-V) characteristics of these three different modules were measured by using a solar simulator (WACOM, WXS-450S-65, AM 1.5 G) with various light concentration ratios at room temperature. An optical rod was used as a secondary optic concentrator to focus the light within the designated cell area under the highly concentrated solar irradiation.

3. Results and discussion

3.1. Design and fabrication of BARCs

Unlike silicon solar cells or any other types of solar cells, III-V based multiple-junction solar cells have an extremely wide absorbing bandwidth that requires well-defined moth eye structures. Previous studies revealed that the grating period of the moth eye structure determines the cut-off band at the short wavelength region and the height of the moth eye structure affects the tail of the high transmission band [21]. From these rules, tapered high aspect-ratio structures are the ideal geometry for broadband antireflection, but are challenging to fabricate on a glass substrate by traditional lithography. The transmittance calculation based on the RCWA method shown in Fig. 2 provides guidance for the selection of period and height of the moth eye structure. In this calculation, hexagonal closely packed (hcp) nanostructures with linearly tapered profile were used, for simplicity, instead of randomly distributed geometry. Upto the fifth diffraction order was considered to calculate the diffraction efficiency of the structures, and total transmittance for all the diffraction order was plotted in Fig. 2. The dispersion relation and the extinction coefficient of borosilicate glass at each wavelength were considered. Since the refractive index of the silicone resin is quite similar to that of the coverglass, only a single-side moth eye structure is needed. As shown in Fig. 2(a), the single-side moth eye structured glasses yield transmittance was ~96% due to the graded refractive index profiles, while it is only ~93% for the flat surface. For the moth eye structure with a period of 200 nm and a height of 500 nm, the transmittance is sustained to high values over a wide wavelength range of 300 - 1800 nm. For the period of 400 and 600 nm, however, an undesirable reduction in the usable spectrum occurs at ~540 nm and 800 nm, respectively, which is caused by the higher order diffraction. Figure 2(b) shows the effect of grating height on the transmittance spectra of single-side moth eye structured glasses. At the height of 200 nm, the transmittance curve is sustained at over 96% at short wavelength regions, however, it decays monotonically as the wavelength increases and then goes down to 95% around 900 nm. As the height increases from 200 nm to 500 nm, the high transmission band (i.e. T > 95%) is increased and this band maintained until the wavelength reaches 1800

#172541 - $15.00 USD Received 23 Aug 2012; revised 21 Sep 2012; accepted 25 Sep 2012; published 15 Oct 2012

nm at the height of 500 nm. This can be explained by the fact that the effective refractive index of a taller feature is more gradually changed.

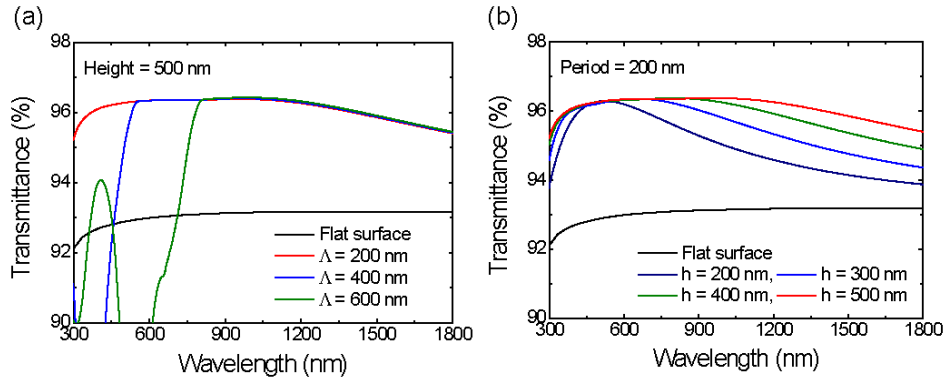

Fig. 2. Calculated total transmittance spectra (300 - 1800 nm) of glasses with moth eye structure (single-side) (a) for 200, 400, and 600 nm period and (b) for 200 - 500 nm heights with 100 nm steps. Transmittance data of glass with a flat surface is also included as a reference.

A sub-200 nm pattern with an aspect ratio of >2 is difficult to obtain through conventional nanolithography, due to the low etch selectivity of glass over e-beam resist or photoresist as well as time consuming fabrication schemes. In contrast, metal NPs act as nano-scale hard masks, and these enable high aspect ratio nano features. Figure 3(a) shows the SEM images of thermally dewetted Ag NPs on coverglass substrates with thicknesses of (i) 10 nm, (ii) 20 nm, and (iii) 30 nm, respectively. The average size of the Ag NPs and the distance of each NP increased as the deposited film thickness increased and these features transferred to the fabricated moth eye structure. After the overall dry etch process of the Ag NPs and the removal of Ag residues, disordered and tapered nanoscale patterns were generated on the coverglass surface. As shown in Fig. 3(a), the pattern height for the moth eye structure with 10 nm thick Ag films was ~500 nm and taller heights are observed in the structure with thicker Ag films. This can be explained by the fact that the packing density affects the etch rate. Figure 3(b) shows the measured transmittance spectra of the base glass and moth eye glasses with different Ag film thicknesses in the wavelengths of 300 - 2400 nm. If the glass has flat surface on both sides, the reflection values are the same for air/glass interface and glass/air interface. In this case, (100-T_{bare}) / 2 means the reflection at single side. Therefore, if the reflection is 0 at one side, the total transmittance can be defined as 100-(100-T_{bare})/2. This maximum transmittance for the glass with zero-reflection at single side is also presented in Fig. 3(b). As expected, transmittance drops exist at the short wavelength ranges for the moth eye structures with 20 and 30 nm Ag films, while the transmittance curve was sustained over the full solar spectral range for those with 10 nm Ag film. These drops are attributed to the large distance between the tapered structures, which generates higher order diffraction. Since the disordered structures consist of multiple spatial wavelength components to the pattern, the curves do not change rapidly, a result that is different than the expected ones in the calculation. In the case of Ag 10 nm, as the wavelength increases, the transmittance decays faster than that of 20 and 30 nm because of their relatively smaller height. Nevertheless, the moth eye structure fabricated with Ag 10 nm on the coverglass is enough to use as BARCs over the range of interest (300 - 1800 nm). The averaged value of transmittance for the case of 10 nm Ag film is 95.7% in the range of 300 - 1800 nm, which is quite similar with the ideal value (T_{max_ave} = 96.5%).

#172541 - $15.00 USD Received 23 Aug 2012; revised 21 Sep 2012; accepted 25 Sep 2012; published 15 Oct 2012

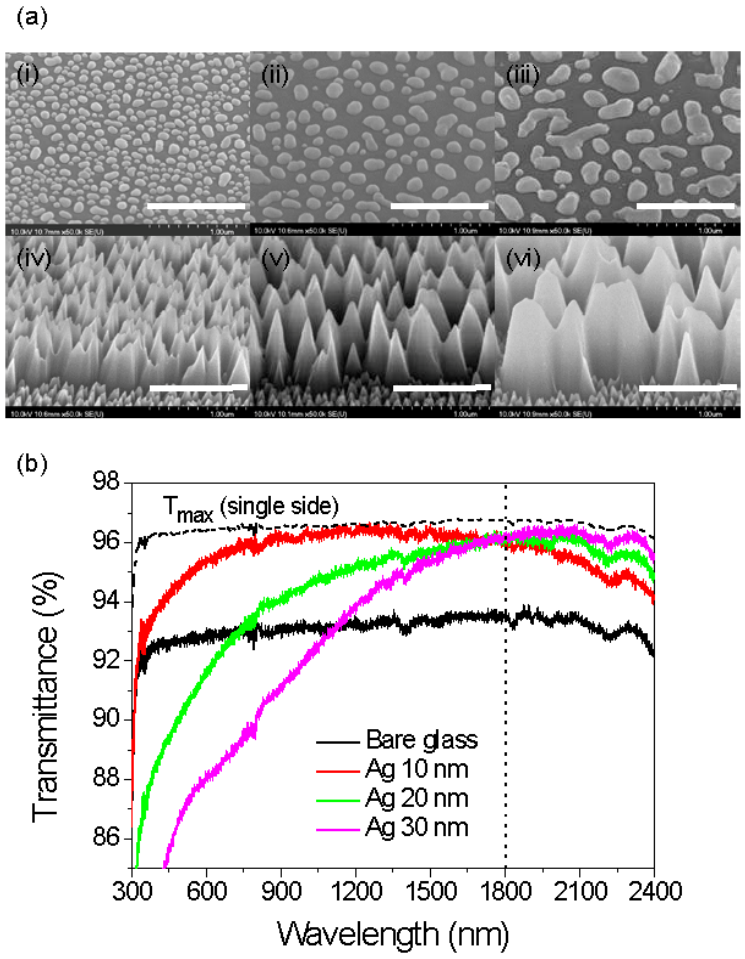

Fig. 3. (a) SEM images (45°-tilted angle view) of (i-iii) thermally dewetted Ag NPs on coverglass substrates and (iv-vi) moth eye structures fabricated with an overall dry etch process for 7 min. Initial Ag film thicknesses correspond to (i, iv) 10 nm, (ii, v) 20 nm, and (iii, vi) 30 nm, respectively. Scale bar: 1 μm. (b) Measured transmittance of a bare glass (black solid line) and moth eye structure integrated glasses with Ag film thickness of 10, 20, and 30 nm, respectively. A black dotted line corresponds to the maximum transmittance spectra of glass with zero-reflectance at single-side.

3.2. III-V based sub-receiver module with BARCs

To verify the effect of BARCs on the cell performance, the BARCs with an Ag film thickness of 10 nm were mounted on InGaP/GaAs/Ge triple-junction solar cells with silicone resin. Figure 4(a) shows the measured reflectance spectra of the cells with three different types (i. e., without BC, with BC, with BARC). In all cases, the reflectance spectra show ripple patterns in the wavelength range above ~900 nm due to the interference of light reflected at the different interfacial layers inside the cell structure, which is analogous to a Fabry-Perot resonance. These fringing on the reflectivity of triple-junction solar cells has similar tendency with the calculation results in other literature [9]. By applying the BC, the reflectance was slightly lowered to the level without BC, owing mainly to the relaxed refractive index gap between air and the cells. As shown in Fig. 4(a), it is clear that the BARC have the lowest reflectance over the whole solar spectral range compared to that of other cases. It is valuable to calculate the solar weight reflectance (SWR), which is determined by the ratio of the reflected photons to total incident photons [22], to optimize the AR structure. The SWR of

#172541 - $15.00 USD Received 23 Aug 2012; revised 21 Sep 2012; accepted 25 Sep 2012; published 15 Oct 2012

BARC for the wavelength of 300 - 1800 nm is 2.11%, which is 3.20% and 4.58% lower than that of the cells with and without the BC, respectively. This reflectance suppression contributes to the enhanced current density of the fabricated sub-receiver module. Figure 4(b) represents the measured current J-V curves for three different types of sub-receiver modules under one-sun of Air Mass (AM) 1.5G. The obtained device characteristics are summarized in Table 1. The values in the brackets represent the data before BC and BARC structures are applied. The sub-receiver module without BC had a short-circuit current density (J_{sc}) of 14.88 mA/cm^2, and this value was enhanced 3.29% by adding the BC. The use of BARC instead of BC brings an additionally improved J_{sc} of 4.99% compared to that of the BC due to the efficient light management, while the open circuit voltage (V_{oc}) and the fill factor were kept at similar values.

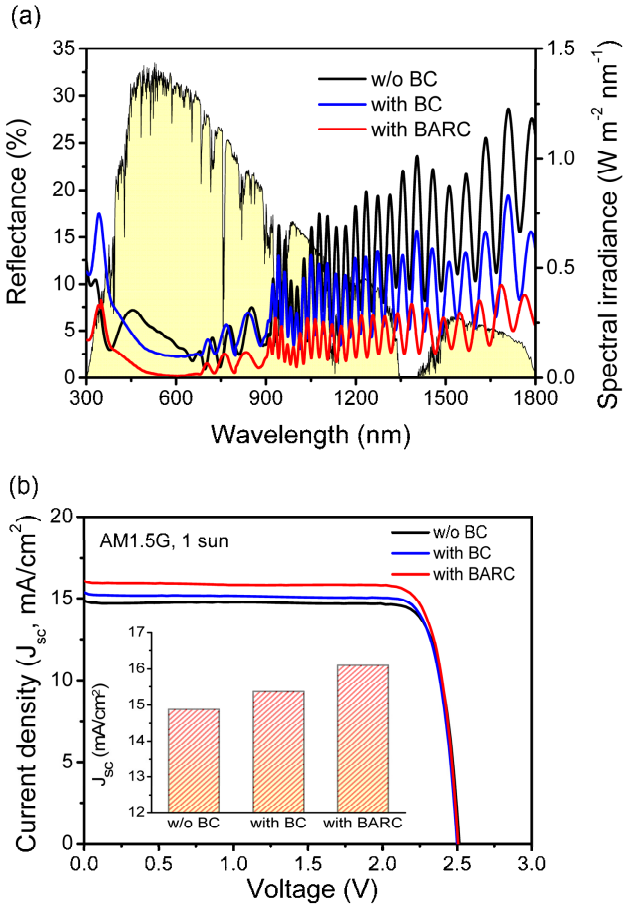

Fig. 4. (a) Measured reflectance results of GaInP/GaAs/Ge triple-junction solar cells without BC (black line), with BC (blue line), with BARC (red line). AM 1.5G solar spectrum is also shown as a reference. (b) J-V characteristics of sub-receiver modules with three different types under AM 1.5G 1-sun. Inset shows the J_{sc} of modules of three types.

Table 1. Device characteristics of the sub-receiver modules for three different types

Types	SWR (%)	V_{oc} (V)	J_{sc} (mA/cm^2)	Fill Factor (%)	Efficiency (%)
Without BC	6.69	2.52	14.88	84.04	31.45
With BC	5.31 (6.39)	2.50 (2.51)	15.37 (14.92)	83.60 (84.25)	32.11 (31.60)
With BARC	2.11 (6.82)	2.51 (2.51)	16.10 (14.73)	83.06 (83.92)	33.52 (31.22)

#172541 - $15.00 USD Received 23 Aug 2012; revised 21 Sep 2012; accepted 25 Sep 2012; published 15 Oct 2012

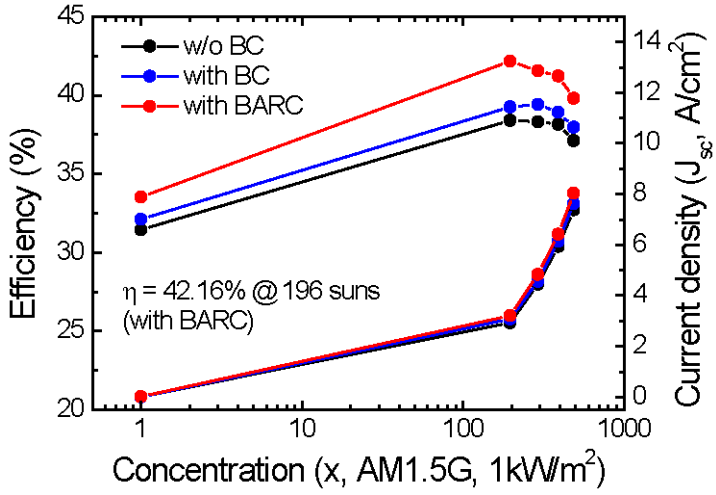

Fig. 5. Power conversion efficiency and current density of CPV sub-receiver modules with three different types as a function of light concentration ratio.

Under the light concentration, the cell efficiency increased due to the increased V_{oc} and fill factor. Figure 5 illustrates the power conversion efficiency and J_{sc} of the CPV sub-receiver modules versus the light concentration ratio. A strong increase in power conversion efficiency was shown in all three curves, and these have a roll-over point at around 200 - 300 suns, which results from the decreased fill factor by the increased series resistance of the cells [23]. The modules with BC and BARC exhibit the improved power conversion performance in comparison to the modules uncovered by glass and resin, which is mainly caused by the increased J_{sc}. The tendency of the enhanced efficiency was sustained at high concentration ratio, and the maximum efficiency of the sub-receiver module with BARC was achieved at 42.16% for 196 suns, which is a 7.41% boosted value, relative to the use of conventional coverglasses.

4. Conclusion

To improve the power conversion efficiency of a III-V based CPV sub-receiver module, the moth eye structures were fabricated on a coverglass substrate using thermally dewetted Ag NPs, and their optical characteristics were investigated in terms of wavelength, together with a theoretical calculation using the RCWA method. The fabricated moth eye structures on the coverglass substrate showed very high transmittance compared to the sample with a flat surface over the full solar spectral range (300 - 1800 nm). Also, the fabricated CPV sub-receiver module with BARCs showed an increased J_{sc} both in one sun and high concentration mode, without any detrimental changes. From these results, we expect that the use of BARCs may provide a promising potential for various photovoltaic devices.

Acknowledgment

This work was partly supported by the National Research Foundation of Korea (NRF) grant funded by the Korea government (MEST) (no. 2011-0017606), by the World Class University (WCU) program at GIST through a grant provided by MEST of Korea (R31-20008-000-10026-0), and by the Core Technology Development Program for Next generation Solar Cells of Research Institute for Solar and Sustainable Energies (RISE), GIST. The authors would like to acknowledge Mr. Sooraj Ravindran in GIST for his fruitful comments and suggestions.

#172541 - $15.00 USD Received 23 Aug 2012; revised 21 Sep 2012; accepted 25 Sep 2012; published 15 Oct 2012